McKee et al. *Journal of Mathematics in Industry* (2016) 6:3
DOI 10.1186/s13362-016-0019-3

Journal of Mathematics in Industry
a SpringerOpen Journal

RESEARCH Open Access

Analytic solutions of a simple advection-diffusion model of an oxygen transfer device

Sean McKee[1], Ewan A Dougall[2] and Nigel J Mottram[1*]

*Correspondence:
nigel.mottram@strath.ac.uk
[1]Department of Mathematics & Statistics, University of Strathclyde, Livingstone Tower, Glasgow, G1 1XH, UK
Full list of author information is available at the end of the article

Abstract

Artificial blood oxygenation is an essential aspect of cardiopulmonary bypass surgery, maintaining physiological levels of oxygen and carbon dioxide in the blood, and thus temporarily replacing the normal function of the lungs. The blood-gas exchange devices used for such procedures have a long history and have had varying degrees of success. In this paper we consider a simple model of a new approach to enhancing the diffusion of oxygen into the blood while it is contained in the artificial blood oxygenator. We show that using a transverse flow, which may be set up using mixing elements that we have previously shown experimentally to enhance blood oxygenation, will increase the oxygen levels within the blood. This simple model and associated analytic solutions can then be used to aid the optimisation of blood oxygenation devices.

Keywords: blood oxygenation; advection diffusion model; mathematical analysis; numerical simulation

1 Artificial blood oxygenation

During cardiopulmonary bypass (CPB) procedures, it is necessary to maintain physiological levels of oxygen and carbon dioxide in the blood. To do this, the patient is connected to a blood-gas exchange device (commonly known as a blood oxygenator) which replaces the respiratory function of the natural lungs. Such devices have a relatively long history, and by the end of the nineteenth century two different methods of organ perfusion had been developed: von Schröder [1] designed a bubble oxygenator in 1882 while in 1885 von Frey and Grubber [2] developed a rotating disc oxygenator. However, probably the first successful device was created by Gibbon [3] who in 1939 produced a vertical screen oxygenator, a variant of which was eventually employed in the first successful clinical cardiopulmonary bypass procedure in 1953 [4]. However, there was general agreement that direct contact between the gas and blood phases, which occurred in these devices, was not conducive to prolonged use surgically. Thus with the advent of polydimethysiloxane (silicon rubber), membrane oxygenators were constructed, initially using a parallel plate configuration, with alternating layers of blood and oxygen, separated by a semi-permeable membrane.

Oxygenator design was further modified by the utilisation of thin-walled hollow fibres (typically 250 μm internal diameter). This version of the oxygenator more closely resem-

bled the capillary beds present in natural lungs. In this design, either blood or oxygen can flow down the hollow fibre, while the other medium flows outside. In the original hollow fibre devices blood was contained within the fibre lumen and they were termed intraluminal flow (ILF) [5, 6]. However, it was found that this configuration required large areas of membrane material (approximately 5.0 m^2 for adult CPB) and that the gas transfer efficiency was limited by the ability of oxygen to diffuse in blood. A further revision of the hollow fibre device therefore had blood flowing through a hollow fibre matrix with oxygen diffusing from within the fibre lumens. This is known as extra-luminal flow (ELF) and was found to be 3-4 times more efficient in gas transfer than ILF due to the advective enhancement of the transport process in the blood phase.

Whichever geometry of oxygenation device used, the process of oxygenation of blood is the same. Oxygen is pumped into the device across a semi-permeable membrane and so enters the blood by being dissolved in the blood plasma. This dissolved oxygen then becomes bound to haemoglobin in the red blood cells through a reaction that occurs at the cell membrane. The take-up of oxygen by the cells is, however, limited and there exists a maximum level of the concentration of bound oxygen. In order to model a blood oxygenation device it is necessary to consider the concentrations of both dissolved and bound oxygen and the effects of advection, diffusion and reaction.

There have been numerous early studies conducted into mathematically and numerically modelling this type of gas transfer (see e.g. [7–16]). These modelling studies have tended to predict greater efficiency with the use of ELF. More recent work includes that of Hewitt et al. [17] who considered an intravenous membrane oxygenator with a pulsating balloon catheter, Suitek and Federspiel [18] who focuses on CO_2 removal, Taskin et al. [16] who considered microscale modelling of blood flow and oxygen transfer and Potkay [19] who produced a limited, but nonetheless closed form solution, thus avoiding the normally extensive numerical computation. More detailed models of gas exchange in the pulmonary capillaries have been explored by Whiteley et al. [20] (see also Whiteley et al. [21]) and Vadapalli et al. [22]. Their models, although closely related, are not directly applicable to artificial lungs (i.e. oxygenators). Furthermore, their models are restricted to a single blood cell, or, in the case of Vadapalli et al., three equidistant blood cells. Other related work on oxygen transfer in blood includes that of Caputo et al. [23] and Formaggia et al. [24] and the references therein although this work largely concentrates on rectilinear flows and considers the nonlinear aspects of the oxygen binding-unbinding reaction kinetics. There is also a vast literature on the analytic and numerical modelling of the flow of blood in physiological situations, for instance with arterial branching and compliant arterial walls (see [25] and references therein). However, in our present situation we are considering an artificial oxygenator with a single capillary and non-compliant walls and therefore significant simplification of the mathematical model is possible.

In recent work [26], we have experimentally considered transverse flow-enhanced oxygenation in a simple oxygenation device. In this situation we used a helical element inserted into a capillary (see Figure 1). This type of mixer element has previously been shown to mix two species within a flow, enhancing diffusive mixing by introducing transverse and angular velocities into the normally rectilinear flow. In [26] we investigated a single capillary, through which either water or blood flowed, and into which oxygen permeated through the semi-permeable membrane that made up the wall of the capillary. The experimental system is sketched in Figure 2. In this experiment the caplliaries were constructed

Figure 1 A typical helical static mixer (Series 120 Disposable Mixing Element, Nordson EFD).

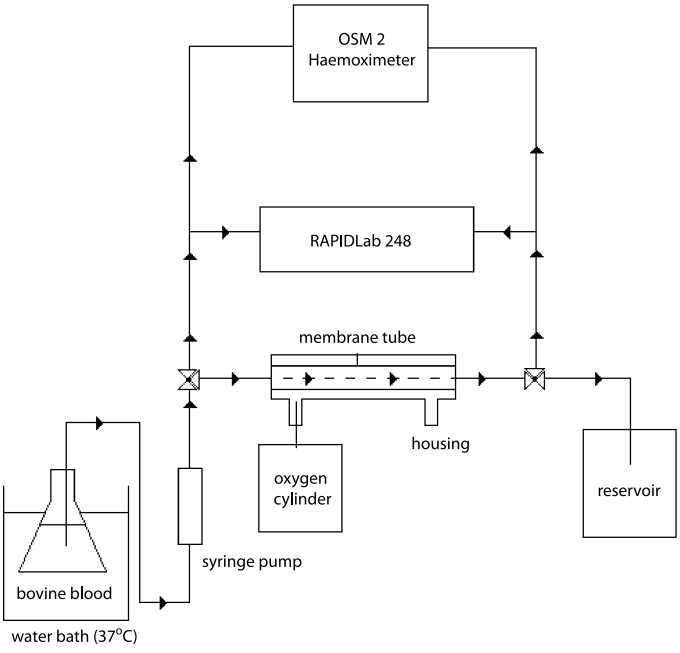

Figure 2 Sketch of the experimental setup for blood flow through a single capillary.

from Celgard 2500, a semi-permeable membrane that can be formed with or without the mixer element included. Twelve devices, six with static mixers and six without, with the mixers coated with Sigmacote in order to prevent blood clots forming on the mixer blades. These capillaries were then housed within a gas-impermeable plastic housing into which oxygen could be introduced and thus enter into the lumen through the semi-permeable membrane.

The blood was heated to 37° and the oxygen levels were raised to physiological venous levels and measured. As indicated in Figure 2, a syringe pump (60 ml JMS SP-100) was used to drive the blood through the membrane. Blood samples were taken at the device entrance and exits via three-way taps. These samples were used to measure the oxygen partial pressure levels (using a Siemens RAPIDLab 248 blood/gas analyser) and the haematocrit and oxygen saturation of the blood (using a Hawksley Micro Haematocrit Centrifuge and a Radiometer OSM-2 Haemoximeter) before and after the blood had passed through the oxygenator. From these measuements the increase in blood oxygen fractional saturation (S, defined below in Section 2) could be calculated. The oxygenator was ventilated with 100% oxygen, at a flow rate of 30 ml min^{-1}. Further experimental details are included in [26].

As testing was performed on single capilliaries, blood flow rates remained at low levels. The blood flow rates were varied between 1 ml min^{-1} and 4 ml min^{-1} in 1 ml min^{-1} increments. Preliminary experiments were conducted with water instead of blood and conclusively showed that the presence of the mixer enhanced the levels of dissolved oxygen. A three dimensional numerical study, included the mixing elements, using COMSOL Multiphysics [27] was also undertaken and agreed very well with the experimental results [26]. It was found that, with no mixing element present, the oxygen transfer from the membrane towards the centre of the lumen was due to diffusion only. However, with a mixing element inserted, the introduction of a transverse flow velocity, from the region of high oxygen concentration at the membrane to low oxygen concentration away from the wall, enhanced the diffusion process and led to greater oxygen levels, of up to 100%, by the time the water had passed through the device. The scaling of this effect was tested by introducing different lengths of mixing elements and, rather than being a mixing phenomena which increased the effective diffusion constant, it was found that the increased oxygenation was due to the advection of oxygen saturated blood from the membrane wall to the centre of the capillary [26].

The same effect also occurred in the blood flow experiments. Figure 3 shows the experimental results, indicating a much more modest increase in oxygen transfer of only around 3%. Even though these results showed that only a limited oxygenation enhancement could occur it was felt that this type of effect, a transverse flow induced increase in oxygen levels, once optimised, could be used to make more efficient and smaller oxygenation devices.

In this paper, inspired by these results, we consider a much more general model of transverse flow enhanced oxygenation, for a planar rather than a cylindrical device. The model presented below is therefore a significant simplification of the experiment described above but contains the essential features: the dominant flow of a liquid in one direction; with a semi-permeable membrane introducing oxygen through diffusion in a direction perpendicular to the flow; together with a transverse flow from the membrane into the main flow region. Through the use of Laplace transforms, analytic and asymptotic solutions are obtained to the resulting advection-diffusion problem. Numerical solutions are obtained for a more complete model, and compared to the analytic and asymptotic solutions. Good agreement between the numerical and analytical solutions suggests the simplifying assumptions are justifiable and leads to the possibility of prediction and optimisation for one type of blood oxygenation device.

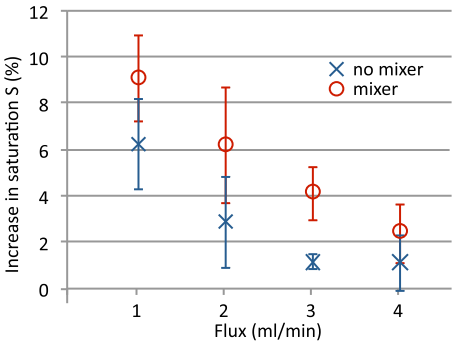

Figure 3 Percentage increase in blood oxygen fractional saturation versus flux through the oxygenator with and without a mixing element.

2 Mathematical modelling

As indicated in the previous section, a model system will be proposed here, and we will consider the concept of transverse flow enhanced oxygen transfer using a parallel plate geometry. In this study therefore, the geometry to be modelled is the quarter plane $x \geq 0$, $z \geq 0$ with an inlet at $z = 0$ and a wall made of a semi-permeable material at $x = 0$, see Figure 4.

For such a system the appropriate mathematical model for the concentration of a substance in a two dimensional geometry can, in general, be modelled by the advection-diffusion-reaction equation,

$$\frac{\partial c}{\partial t} + u\frac{\partial c}{\partial x} + w\frac{\partial c}{\partial z} = D\left(\frac{\partial^2 c}{\partial x^2} + \frac{\partial^2 c}{\partial z^2}\right) + f(c), \tag{1}$$

where $c(x, z, t)$ is the concentration, D the diffusion coefficient, $f(c)$ the reaction rate function and $\mathbf{u} = (u, w)$ is the two dimensional fluid velocity. The reaction function $f(c)$ contains terms that model the introduction and the removal of the material. The second and third term in equation (1) represent the advection of material caused by the fluid flow in the x- and z-directions, respectively.

Equations of this type have been used to model a vast array of real-world problems where the concentration of a dissolved substance evolves in time because of diffusion, advection by the flow of the background liquid, and the point-wise increase or the decrease of the concentration level from a source/sink term. Of particular note in the present context, are those applications where the introduction of the substance occurs at a semi-permeable boundary. In soil science, for instance, the rate at which a chemical constituent moves through soil is determined by several transport mechanisms: advection, diffusion, dispersion, adsorption and zero-order or first-order production and decay. Van Genuchten and Alves [28] have provided a substantial compendium of analytic solutions to a wide range of problems in soil science. A more recent paper by Yuan and Lu [29] deals with an analytic solution to vertical flow in unsaturated, rooted soils with variable surface fluxes; the article contains an extensive list of references. Another relevant area is the transport of partic-

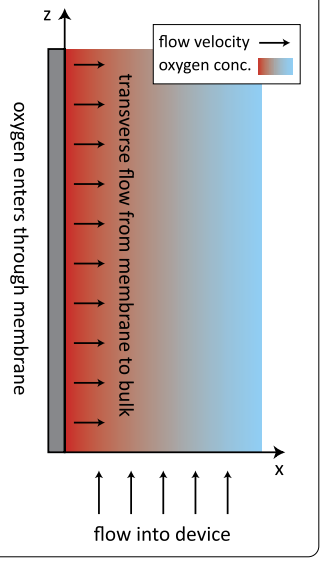

Figure 4 Schematic representations of the device geometry: Deoxygenated blood (or blood with a low oxygen content) flows into the device at $z = 0$ while oxygen is pumped through a wall located at $x = 0$, made of a semi-permeable membrane.

ulate matter (pollution) through the atmosphere with deposition at ground level: McKay et al. [30], for instance, developed an analytic solution through Laplace transforms and contour integration. More recently, interesting analytic solutions have been obtained by Kumar et al. [31] and Jaiswal and Kumar [32] for the one-dimensional advection-diffusion equation with a variable diffusion coefficient and a variable velocity in both a finite and infinite domain. In a biological setting, an application also arises from drug diffusion through tissue. In the case of drug-eluting stents the pressure difference between the lumen and the surrounding tissue means that advection also plays a role. McGinty et al. [33] produced an analytic solution; mathematically this was interesting as the inverse Laplace transform contained three branch points. Pontrelli and de Monte [34], on the other hand, considered the problem of drug diffusion through multiple layers and obtained analytic solutions using a separation of variables approach.

This short list of similar systems in which a concentration influx occurs at the boundary (i.e. from the soil surface or drug-eluting stent) leads to a type of mixed boundary condition that is similar to the situation we consider in this paper. Here we find that this set of equations is in fact analytically solvable through the application of Laplace transforms and can be simplified in some limiting, but physically relevant, cases to provide information which may be used to inform device construction and optimisation.

In general, for a Newtonian fluid the velocity and pressure may be found by solving the Navier-Stokes equations for the conservation of momentum, coupled with the mass conservation equation. However, blood is not Newtonian: the flow profile is known to be much closer to plug flow than Poiseuille flow. If the device is not too small then 'Newtonian' plug flow with a fixed (effective) viscosity is not an unreasonable model [35]. Thus, we shall simply consider a constant form of the fluid flow in the z-direction, $w = \bar{w}$, $x > 0$. Furthermore, in this study we have also included an effective component of velocity in the x-direction, $\bar{u}$. Since we are aiming to demonstrate the influence of a transverse flow in general, rather than through a specific realisation, we take a simplified approach. Therefore, although normally the geometric form of the mixer, such as a solid helical screw-type element, will introduce fully three-dimensional flow, we will replace the mixer with a constant component of velocity in the x-direction. The two non-zero constant components of velocity, therefore, will be taken to be

$$u = \bar{u}, \qquad w = \bar{w}, \quad \text{for } x, z > 0. \tag{2}$$

The assumption of constant flow velocity is a significant simplification and the correct form of the flow, a solution to the Navier-Stokes equations together with the mass conservation equation, would affect the concentrations through the convective term in Eq. (1). However, under the assumption that the flow is almost plug-like, and in order to obtain analytic solutions so that we may derive a predictive model for use in the optimisation of the device, we will continue with this constant velocity model.

In this study, in addition to the fluid velocity, we shall model two coupled concentrations: c_b, the concentration of oxygen bound to haemoglobin, and c_d, the concentration of dissolved oxygen in the system. There are, therefore, two concentration equations coupled through a reaction function $f(c_b, c_d)$. This function models the reaction whereby dissolved oxygen and haemoglobin combine to produce oxygen bound to haemoglobin, as well as the reverse reaction whereby bound oxygen reverts to dissolved oxygen. From equation (1),

the two concentration equations may be written as

$$\frac{\partial c_b}{\partial t} + u\frac{\partial c_b}{\partial x} + w\frac{\partial c_b}{\partial z} = D_b\left(\frac{\partial^2 c_b}{\partial x^2} + \frac{\partial^2 c_b}{\partial z^2}\right) + f(c_b, c_d), \tag{3}$$

and

$$\frac{\partial c_d}{\partial t} + u\frac{\partial c_d}{\partial x} + w\frac{\partial c_d}{\partial z} = D_d\left(\frac{\partial^2 c_d}{\partial x^2} + \frac{\partial^2 c_d}{\partial z^2}\right) - f(c_b, c_d), \tag{4}$$

where the reaction term is of opposite sign in the two equations because oxygen is neither lost nor created during the reaction: that is, oxygen either changes from dissolved to bound or the reverse. The two diffusion coefficients, D_b and D_d, denote, respectively, the diffusion coefficients in blood for the concentration of oxygen bound to haemoglobin and the concentration of dissolved oxygen.

In almost all the previous studies of such a system mentioned above [7–16, 36] the problem is solved numerically, and some assume the flow in the direction normal to the main pressure-driven flow is small, i.e. $\bar{u} = 0$. We shall not make this assumption. Rather, we shall make the very reasonable assumption that bound oxygen is primarily transported by advection, rather than diffusion, that is, $D_b = 0$.

It is usual in this field (e.g. [37]) to consider partial pressure of the dissolved oxygen, P_{O_2}, rather than the concentration, c_d. Following this convention, the equation for c_d will be replaced by one for the partial pressure using the relationship

$$c_d = \alpha_{O_2} P_{O_2},$$

where α_{O_2} is the solubility of oxygen in blood. With these assumptions equations (3) and (4) become

$$\frac{\partial c_b}{\partial t} + u\frac{\partial c_b}{\partial x} + w\frac{\partial c_b}{\partial z} = f(c_b, \alpha_{O_2} P_{O_2}) \tag{5}$$

and

$$\frac{\partial P_{O_2}}{\partial t} + u\frac{\partial P_{O_2}}{\partial x} + w\frac{\partial P_{O_2}}{\partial z} = D_d\left(\frac{\partial^2 P_{O_2}}{\partial x^2} + \frac{\partial^2 P_{O_2}}{\partial z^2}\right) - \frac{1}{\alpha_{O_2}} f(c_b, \alpha_{O_2} P_{O_2}). \tag{6}$$

It is important to consider the timescale of the reaction term $f(c_b, \alpha_{O_2} P_{O_2})$ which describes the process of dissolved oxygen becoming bound and vice versa. It is often assumed that the forward and reverse reactions are sufficiently fast that an equilibrium between dissolved and bound oxygen occurs effectively instantaneously [37]. An empirical relationship between c_b and P_{O_2} is then assumed from experimental data. With this relationship it is then only necessary to solve one of the two equations (5) and (6). The remaining variable is then determined from the empirical relationship.

One commonly used form for this empirical relationship is the Hill formula [38], which assumes that n molecules of dissolved oxygen combine with a single molecule of haemoglobin to form a single molecule of oxygenated haemoglobin. The steady state expression for the amount of bound oxygen can then be obtained from

$$c_b = c_{\max}\left(\frac{P_{O_2}^n}{P_{O_2}^n + P_{0.5}^n}\right), \tag{7}$$

where $P_{0.5}$ is the partial pressure of dissolved oxygen when half of the haemoglobin is saturated. In deriving this expression it is assumed that the haemoglobin can become saturated, that is we can define a maximum concentration of bound oxygen, $c_{\max}$, such that $c_{\max} = \beta_{O_2} c_{Hb}$ where β_{O_2} is the oxygen carrying capacity of haemoglobin and c_{Hb} is the concentration of haemoglobin present in the blood. In equation (7) n can either be assumed to be a model variable or found empirically. In a single reaction the number of molecules of oxygen binding to the haemoglobin may be between one and four and the empirically derived value (around $n = 2.8$ - see e.g. [38]) is a stochastic average of many reactions.

The fractional saturation,

$$S(P_{O_2}) = \frac{c_b}{c_{\max}} = \left(\frac{P_{O_2}^n}{P_{O_2}^n + P_{0.5}^n} \right), \tag{8}$$

is frequently employed as a dependent variable [37]. Therefore, by assuming the steady state form of equations (5) and (6) and introducing the expression for the fractional saturation we obtain

$$c_{\max} \left(u \frac{\partial S}{\partial x} + w \frac{\partial S}{\partial z} \right) = f(c_{\max} S, \alpha_{O_2} P_{O_2}) \tag{9}$$

and

$$u \frac{\partial P_{O_2}}{\partial x} + w \frac{\partial P_{O_2}}{\partial z} = D_d \left(\frac{\partial^2 P_{O_2}}{\partial x^2} + \frac{\partial^2 P_{O_2}}{\partial z^2} \right) - \frac{1}{\alpha_{O_2}} f(c_{\max} S, \alpha_{O_2} P_{O_2}). \tag{10}$$

Since S is a function of P_{O_2} we may write equation (9) in the form

$$c_{\max} \frac{\partial S}{\partial P_{O_2}} \left(u \frac{\partial P_{O_2}}{\partial x} + w \frac{\partial P_{O_2}}{\partial z} \right) = f(c_{\max} S, \alpha_{O_2} P_{O_2}), \tag{11}$$

which may be employed to eliminate the reaction term in (10) to obtain

$$\left(1 + \frac{c_{\max}}{\alpha_{O_2}} \frac{\partial S}{\partial P_{O_2}} \right) \left(u \frac{\partial P_{O_2}}{\partial x} + w \frac{\partial P_{O_2}}{\partial z} \right) = D_d \left(\frac{\partial^2 P_{O_2}}{\partial x^2} + \frac{\partial^2 P_{O_2}}{\partial z^2} \right). \tag{12}$$

This is now the sole governing equation for the system with the flow velocity (u, w) given by (2) and the expression for S given by equation (8).

In order to solve this governing equation, boundary conditions for the dependent variable will need to be specified. At the inflow end of the device, where $z = 0$, it is assumed that there the blood enters with a fixed partial pressure of dissolved oxygen, $P_{O_2} = P_i$. At the blood-oxygenating membrane interface we assume that the flux of dissolved oxygen into the region is due to the injection of oxygen through the membrane,

$$\frac{\partial P_{O_2}}{\partial x} - u P_{O_2} = -\frac{D_m \alpha_m}{D_d \alpha_{O_2} \tau} (P_g - P_{O_2}), \quad x = 0, \tag{13}$$

which is the standard Fickian model for the injection of a chemical through a membrane where D_m is the diffusion coefficient for oxygen in the membrane, α_m is the solubility of

oxygen in the membrane, τ denotes the thickness of the membrane and P_g is the membrane O_2 partial pressure. However, since a semi-permeable membrane is used, through which there is no flow of blood, the velocity is zero and we obtain

$$\frac{\partial P_{O_2}}{\partial x} = -\frac{D_m \alpha_m}{D_d \alpha_{O_2} \tau}(P_g - P_{O_2}), \quad x = 0. \tag{14}$$

The wall Sherwood number,

$$Sh = \frac{D_m \alpha_m L}{D_d \alpha_{O_2} \tau}, \tag{15}$$

where L is a typical lengthscale in the x-direction, is often employed so that (14) may be re-expressed as

$$\frac{\partial P_{O_2}}{\partial x} = -\frac{Sh}{L}(P_g - P_{O_2}), \quad x = 0. \tag{16}$$

To simplify the analysis of this equation we will non-dimensionalise appropriate variables and parameters. We will use the lengthscale L introduced in equation (15) (and which will later be specified as a typical device width) to rescale both $x = L\tilde{x}$ and $z = L\tilde{z}$. The partial pressure could be scaled with a number of quantities but we choose to scale it with $P_{\max} = c_{\max}/\alpha_{O_2}$, the effective maximum partial pressure of bound oxygen, so that $c = P_{O_2}/P_{\max}$.

Through these scalings the following non-dimensional parameters appear: the constant ratio of typical x-component to z-component flow speeds, $\nu = \bar{u}/\bar{w}$; a ratio of diffusive and advective terms, $\delta = D_d/L\bar{w}$; and the rescaled partial pressures, $c_{0.5} = P_{0.5}/P_{\max}$, $c^* = P_g/P_{\max}$, $c_0 = P_i/P_{\max}$.

We therefore obtain the governing equation for the scaled partial pressure of dissolved oxygen in the region $\tilde{x} > 0$, $\tilde{z} > 0$:

$$\left(1 + \frac{\partial S}{\partial c}\right)\left(\nu \frac{\partial c}{\partial \tilde{x}} + \frac{\partial c}{\partial \tilde{z}}\right) = \delta\left(\frac{\partial^2 c}{\partial \tilde{x}^2} + \frac{\partial^2 c}{\partial \tilde{z}^2}\right), \tag{17}$$

where the fractional saturation is given by

$$S(c) = \left(\frac{c^n}{c^n + c_{0.5}^n}\right) \tag{18}$$

and the boundary conditions are

$$\frac{\partial c}{\partial \tilde{x}} = -Sh\left(c^* - c\right), \quad \tilde{x} = 0, \tag{19}$$

$$c = c_0, \quad \tilde{z} = 0. \tag{20}$$

At this point it is important to note that the boundary conditions (19) and (20) are incompatible at $\tilde{x} = 0$, $\tilde{z} = 0$. This indicates that the constraint (20) is unphysical. However, the analysis in the following sections allows a solution to be obtained even with this incompatibility. In fact, the numerical scheme to solve these equations has little difficulty

Table 1 Values of dimensional and non-dimensional parameters

Dimensional Parameters	Symbol	Value	Dimensions
Geometry			
Lengthscale of device	L	2×10^{-3}	m
Oxygen/Haemoglobin			
Diffusion coefficient	D_d	1.5×10^{-9}	$m^2 s^{-1}$
Solubility of O_2 in blood	α_{O_2}	9.98×10^{-6}	mol $m^{-3} Pa^{-1}$
Oxygen binding capacity	β_{O_2}	5.98×10^{-2}	mol kg^{-1}
Haemoglobin concentration	c_{Hb}	120	kg m^{-3}
Maximum bound concentration	$c_{\max}$	7.176	mol m^{-3}
Max. part. press. of bound conc.	$P_{\max}$	7.19×10^5	Pa
Part. press. of half saturation	$P_{0.5}$	3.2×10^3	Pa
Index constant	n	2.8	
Boundaries			
Average longitudinal velocity	$\bar{w}$	4×10^{-5}	m s^{-1}
Average transverse velocity	$\bar{u}$	1×10^{-6}	m s^{-1}
Inlet O_2 partial pressure	P_i	5×10^3	Pa
Membrane O_2 partial pressure	P_g	20×10^3	Pa

Non-dimensional parameters	Symbol	Value
Oxygen/Haemoglobin		
Ratio of diffusion/advection	δ	1.875×10^{-2}
Boundaries		
Ratio of velocities	ν	0.025
Scaled inlet O_2 partial pressure	c_0	0.70×10^{-2}
Scaled membrane O_2 part. press.	c^*	2.78×10^{-2}
Scaled part. press. of half sat.	$c_{0.5}$	0.45×10^{-2}
Wall Sherwood number	Sh	50
Inlet correction parameter	ϵ	1×10^{-3}

in finding an approximate solution, although errors can be large at $x = 0$, $z = 0$. This may be overcome in the numerical scheme by regularisation: replacing the condition (20) with $c = c_0(\tilde{x})$, where $c_0(\tilde{x})$ is a function which is compatible with the boundary condition (19) at $\tilde{x} = 0$. Later we specify a particular form of this boundary condition,

$$c = c_0(\tilde{x}) = c_0\left(1 + \epsilon \exp\left(-\frac{Sh(c^* - c_0(1+\epsilon))}{\epsilon c_0}\tilde{x}\right)\right), \quad \tilde{z} = 0, \tag{21}$$

which is valid for any value of ϵ, termed the inlet correction parameter, in order to compute and plot the numerical solution. As we shall see later, even though the analytic solution must retain the unphysical condition (20) there is very good agreement between this and the numerical solution which uses the regularised condition (21).

The essential dimensional parameters that govern the system are provided in Table 1. These may then be used to obtain the set of non-dimensional parameters required for the solution of the equations (17), (18), (19) and (21). These equation will later be solved numerically using the software package COMSOL Multiphysics [27]. However, as we shall see in the next section, progress can be made analytically using a slightly simplified model.

2.1 A simplified model

We shall make two further assumptions so that we can employ the analytic expressions of the next section. These assumptions are justified below and also allow us to obtain useful qualitative (and quantitative) results which, possibly surprisingly, compare favourably with the numerical results of the model for the oxygenator device.

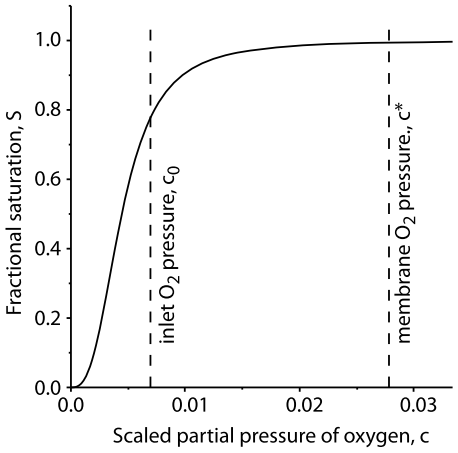

Figure 5 Fractional saturation, *S*, as a function of the non-dimensionalised partial pressure of oxygen *c*. The inlet and membrane pressures c_0 and c^* are indicating the validity of the assumption that S is approximately constant.

We first assume that diffusion in the z-direction, parallel to the membrane, is negligible in comparison with advection in that direction. This is a common assumption in such devices due to the speed at which blood must be flowed through the device in order to mimic the flow in a human body.

The second assumption is that the effective diffusion coefficient in equation (17), $\delta/(1 + \partial S/\partial c)$, is approximately constant, and equal to δ, for the range of concentrations to be considered. This is certainly a reasonable assumption as can be seen from Figure 5, since the fractional saturation will, in our device, be bounded below by the scaled inlet partial pressure c_0 which corresponds to around 80% saturation.

With these assumptions (and removing ˜ for ease of presentation) our simplified non-dimensional model is the following:

$$\nu\frac{\partial c}{\partial x} + \frac{\partial c}{\partial z} = \delta\frac{\partial^2 c}{\partial x^2}, \quad (x,z) \in (0,\infty)\times(0,\infty), \tag{22}$$

subject to

$$c = c_0, \qquad z = 0, \tag{23}$$

$$\frac{\partial c}{\partial x} = -Sh\big(c^* - c\big), \quad x = 0, \tag{24}$$

and assuming that

$$c(x,z) \quad \text{remains bounded for all } x, z. \tag{25}$$

3 Analysis of the advection-diffusion problem

In this section we shall employ Laplace transforms to obtain an analytic solution to the model specified by Eqs. (22-25); in addition some asymptotic forms are provided.

On taking Laplace transforms of equation (22) with respect to the variable z we obtain

$$\delta\frac{d^2\bar{c}}{dx^2}(x,s) - \nu\frac{d\bar{c}}{dx}(x,s) - s\bar{c}(x,s) = -c_0, \tag{26}$$

where

$$\bar{c}(x,s) = \int_0^\infty e^{-zs} c(x,z)\, dz,$$

and condition (23) has been used.

The ordinary differential equation (26) may then be solved to give

$$\bar{c}(x,s) = \frac{c_0}{s} + A(s)\exp\left[\frac{x}{2\delta}\left(\nu + \sqrt{\nu^2 + 4s\delta}\right)\right] + B(s)\exp\left[\frac{x}{2\delta}\left(\nu - \sqrt{\nu^2 + 4s\delta}\right)\right],$$

where $A(s)$ and $B(s)$ are independent of x, but may be functions of the Laplace transform variable, s. Boundedness (25) then implies

$$\bar{c}(x,s) = \frac{c_0}{s} + B(s)\exp\left[\frac{x}{2\delta}\left(\nu - \sqrt{\nu^2 + 4s\delta}\right)\right]. \tag{27}$$

Taking Laplace transforms of (24) (with respect to z) yields

$$\frac{d\bar{c}}{dx}(x,s) = -Sh\left(\frac{c^*}{s} - \bar{c}(x,s)\right) \quad \text{at } x = 0,$$

which, with (27), results in

$$B(s) = \frac{2\delta Sh(c^* - c_0)}{[\sqrt{\nu^2 + 4s\delta} + 2\delta Sh - \nu]s}.$$

Therefore, the solution in Laplace transform space becomes

$$\bar{c}(x,s) = \frac{c_0}{s} + \frac{2\delta Sh(c^* - c_0)}{[\sqrt{\nu^2 + 4s\delta} + 2\delta Sh - \nu]s}\exp\left[\frac{x}{2\delta}\left(\nu - \sqrt{\nu^2 + 4s\delta}\right)\right]. \tag{28}$$

To invert this Laplace transform we shall require the following lemmas:

Lemma 1

$$L^{-1}\left[\frac{1}{\sqrt{s-a}+b}\right] = e^{az}\left(\frac{1}{\sqrt{\pi z}} - be^{b^2 z}\operatorname{erfc}(b\sqrt{z})\right).$$

Lemma 2

$$L^{-1}\left[\frac{1}{s}\exp\left(-\sqrt{a(s+b)}\right)\right] = \frac{1}{2}\left[e^{-\sqrt{ab}}\operatorname{erfc}\left(-\sqrt{bz} + \frac{1}{2}\sqrt{\frac{a}{z}}\right) + e^{\sqrt{ab}}\operatorname{erfc}\left(\sqrt{bz} + \frac{1}{2}\sqrt{\frac{a}{z}}\right)\right].$$

The first of these Lemmas is standard and may be found in, for example, [39] while the second is given by McGinty et al. [40].

Noting that,

$$\frac{1}{\sqrt{\nu^2+4s\delta}+2\delta Sh-\nu}=\frac{1}{2\sqrt{\delta}}\frac{1}{\sqrt{s+\nu^2/4\delta}+\frac{2\delta Sh-\nu}{2\sqrt{\delta}}},$$

and identifying $a := -\nu^2/4\delta$ and $b := \frac{2\delta Sh-\nu}{2\sqrt{\delta}}$ in Lemma 1 yields

$$\begin{aligned}&L^{-1}\left[\frac{1}{\sqrt{\nu^2+4s\delta}+2\delta Sh-\nu}\right]\\&\quad=\frac{1}{2\sqrt{\delta}}\exp\left(-\frac{\nu^2 z}{4\delta}\right)\left(\frac{1}{\sqrt{\pi z}}-\gamma e^{\gamma^2 z}\operatorname{erfc}(\gamma\sqrt{z})\right),\end{aligned}\tag{29}$$

where we have set $\gamma = b = (2\delta Sh-\nu)/(2\sqrt{\delta})$.

Now we note that,

$$\begin{aligned}&\frac{1}{s}\exp\left[\frac{x}{2\delta}\left(\nu-\sqrt{\nu^2+4s\delta}\right)\right]\\&\quad=\exp\left(\frac{\nu x}{2\delta}\right)\frac{1}{s}\exp\left[-\sqrt{\frac{x^2}{\delta}\left(s+\frac{\nu^2}{4\delta}\right)}\right],\end{aligned}$$

and identify $a := x^2/\delta$ and $b := \nu^2/4\delta$ in Lemma 2 so that

$$L^{-1}\left[\frac{1}{s}\exp\left[\frac{x}{2\delta}\left(\nu-\sqrt{\nu^2+4s\delta}\right)\right]\right]\tag{30}$$

$$\begin{aligned}&=\frac{1}{2}\exp\left(\frac{\nu x}{2\delta}\right)\left\{\exp\left(-\frac{\nu x}{2\delta}\right)\operatorname{erfc}\left(-\frac{\nu}{2}\sqrt{\frac{z}{\delta}}+\frac{x}{2\sqrt{\delta z}}\right)\right.\\&\quad\left.+\exp\left(\frac{\nu x}{2\delta}\right)\operatorname{erfc}\left(\frac{\nu}{2}\sqrt{\frac{z}{\delta}}+\frac{x}{2\sqrt{\delta z}}\right)\right\}\\&=\frac{1}{2}\left\{\operatorname{erfc}\left(\frac{x-\nu z}{2\sqrt{\delta z}}\right)+\exp\left(\frac{\nu x}{\delta}\right)\operatorname{erfc}\left(\frac{x+\nu z}{2\sqrt{\delta z}}\right)\right\}.\end{aligned}\tag{31}$$

Thus, by convolution, we obtain

$$\begin{aligned}c(x,z)=c_0+\frac{\sqrt{\delta}}{2}Sh\left(c^*-c_0\right)&\int_0^z\exp\left(-\frac{\nu^2 u}{4\delta}\right)\\&\times\left\{\frac{1}{\sqrt{\pi u}}-\gamma\exp\left(\gamma^2 u\right)\operatorname{erfc}(\gamma\sqrt{u})\right\}\\&\times\left\{\operatorname{erfc}\left(\frac{x-\nu(z-u)}{2\sqrt{\delta(z-u)}}\right)+\exp\left(\frac{\nu x}{\delta}\right)\operatorname{erfc}\left(\frac{x+\nu(z-u)}{2\sqrt{\delta(z-u)}}\right)\right\}du.\end{aligned}\tag{32}$$

The analytic solution given in (32) involves an integral that may be numerically calculated. However, in certain asymptotic limits the integration can be achieved straightforwardly and useful analytic solutions can be obtained.

3.1 Large Sherwood number

One important limit occurs when the membrane oxygen pressure is high so that it is not limited significantly by the diffusion of oxygen away from the wall in the blood. In this

case we may assume that the Sherwood number is large, i.e. $Sh \gg 1$, which, from Table 1, we see is certainly the case here. We may tackle this limiting case in two ways: return to the original model equations and assume that $Sh \gg 1$; or consider the solution of the full problem with $Sh \gg 1$. In the first situation we consider again the problem defined by (22)-(25). As $Sh \to \infty$, the boundary condition (24) becomes

$$c = c^* \quad \text{at } x = 0. \tag{33}$$

Solving the problem (22), (23), (25) and (33), again using Laplace transforms, results in

$$\bar{c}(x,s) = \frac{c_0}{s} + \frac{(c^* - c_0)}{s} \exp\left(\frac{x}{2\delta} \left(\nu - \sqrt{\nu^2 + 4s\delta} \right) \right), \tag{34}$$

where $\bar{c}(x,s)$ is the solution in Laplace transform space. Using the results of the previous subsection allows us to invert (34) to find the solution

$$c(x,z) = c_0 + \frac{1}{2}(c^* - c_0) \left\{ \operatorname{erfc}\left(\frac{x - \nu z}{2\sqrt{\delta z}} \right) + \exp\left(\frac{x\nu}{\delta} \right) \operatorname{erfc}\left(\frac{x + \nu z}{2\sqrt{\delta z}} \right) \right\}. \tag{35}$$

Alternatively we may consider the solution to the full problem (31) with $Sh \to \infty$. We first consider the function

$$f(x) = \sqrt{\delta} Sh \exp\left(-\frac{\nu^2 x}{4\delta} \right) \left(\frac{1}{\sqrt{\pi x}} - \gamma e^{\gamma^2 x} \operatorname{erfc}(\gamma \sqrt{x}) \right) \tag{36}$$

which forms part of the full solution. We will now show that this function behaves as a delta function as $Sh \to \infty$, i.e. that,

$$\int_0^\infty f(x)\, dx \to 1 \quad \text{as } Sh \to \infty, \tag{37}$$

$$f(0) \quad \text{is finite as } Sh \to \infty, \tag{38}$$

$$f(x) \to 0 \quad \text{for all fixed } x > 0, \text{ as } Sh \to \infty. \tag{39}$$

We first consider (37)

$$\begin{aligned} \lim_{Sh\to\infty} \int_0^\infty f(x)\, dx &= \lim_{Sh\to\infty} \sqrt{\delta} Sh \left\{ \int_0^\infty \frac{\exp(-\frac{\nu^2 x}{4\delta})}{\sqrt{\pi x}}\, dx \right. \\ &\quad \left. - \gamma \int_0^\infty \exp\left(\left(\gamma^2 - \frac{\nu^2}{4\delta} \right) x \right) \operatorname{erfc}(\gamma \sqrt{x})\, dx \right\} \\ &= \lim_{Sh\to\infty} \sqrt{\delta} Sh \{ I_1 - I_2 \}. \end{aligned}$$

Now, $I_1 = (2\sqrt{\delta})/\nu$ using the fact that

$$\int_0^\infty x^{-1/2} e^{-x}\, dx = \Gamma\left(\frac{1}{2} \right) = \sqrt{\pi}. \tag{40}$$

To evaluate the second integral it is first necessary to interchange the order of integration and then use the definition of the gamma function (40) to obtain

$$I_2 = \frac{\gamma}{(\gamma^2 - \nu^2/4\delta)}\left(\frac{2\sqrt{\delta}\gamma}{\nu} - 1\right). \tag{41}$$

Thus

$$\lim_{Sh\to\infty}\int_0^\infty f(x)\,dx = \lim_{Sh\to\infty}\sqrt{\delta}Sh\left\{\frac{2\sqrt{\delta}}{\nu} - \frac{2\gamma^2\sqrt{\delta}}{\nu(\gamma^2 - \nu^2/4\delta)} + \frac{\gamma}{(\gamma^2 - \nu^2/4\delta)}\right\}$$
$$= 1,$$

since $\gamma \to \sqrt{\delta}Sh$ as $Sh \to \infty$.

Let us now consider $x > 0$ and $Sh \gg 1$, (39). Using the large argument expansion of the error function complement [41]

$$\operatorname{erfc}(z) \sim \frac{e^{-z^2}}{\sqrt{\pi}z}\left(1 - \frac{1}{2z^2}\right) \quad \text{as } z \to \infty, \tag{42}$$

we observe that

$$f(x) \sim \gamma\left(\frac{1}{\sqrt{\pi x}} - \frac{1}{\sqrt{\pi x}}\left(1 - \frac{1}{2\gamma^2 x}\right)\right),$$

since $\sqrt{\delta}Sh \sim \gamma$ as $Sh \gg 1$. Thus $f(x) \sim 0$ as $\gamma \to \infty$ for any fixed value of $x > 0$.

The case '$x = 0$', (38), is a little more subtle. There are really two limits: $Sh \to \infty$ and $x \to 0$; and we need to prescribe how fast they tend to their respective limits. We consider the distinguished limit where $xSh \to 1$ as $x \to 0$, or equivalently $\gamma x \to \sqrt{\delta}$. This allows the problem to be reduced to one with a single limit:

$$\lim_{\substack{x\to 0\\ Sh\to\infty\\ xSh\to 1}} f(x) = \lim_{x\to 0}\frac{\sqrt{\delta}}{x}e^{-\nu^2 x/4\delta}\left\{\frac{1}{\sqrt{\pi x}} - \frac{\sqrt{\delta}}{x}e^{\delta/x}\operatorname{erfc}\left(\frac{\sqrt{\delta}}{\sqrt{x}}\right)\right\},$$

which, upon using (42), we see is, in fact, zero.

Thus we have shown that the function $f(x)$, given by (36) satisfies the three conditions, (37)-(39) and so, in the limit of large Sherwood number, behaves like a delta function. Because of this we may simplify (32) so that

$$\lim_{Sh\to\infty} c(x,z) = c_0 + \frac{1}{2}(c^* - c_0)\left\{\operatorname{erfc}\left(\frac{x - \nu z}{2\sqrt{\delta z}}\right) + e^{\nu x/\delta}\operatorname{erfc}\left(\frac{x + \nu z}{2\sqrt{\delta z}}\right)\right\}, \tag{43}$$

as in (35).

Figure 6 compares the exact analytic solution for the simplified model, (32), the solution in the limit of large Sherwood number, (35), and the numerical solution to the full model (17), (18), (19) and (21). For this numerical solution we have used the software package COMSOL Multiphysics [27]. COMSOL uses a relatively standard finite element approach (a direct nonlinear solver of the stationary system) and, due to the simplicity of the do-

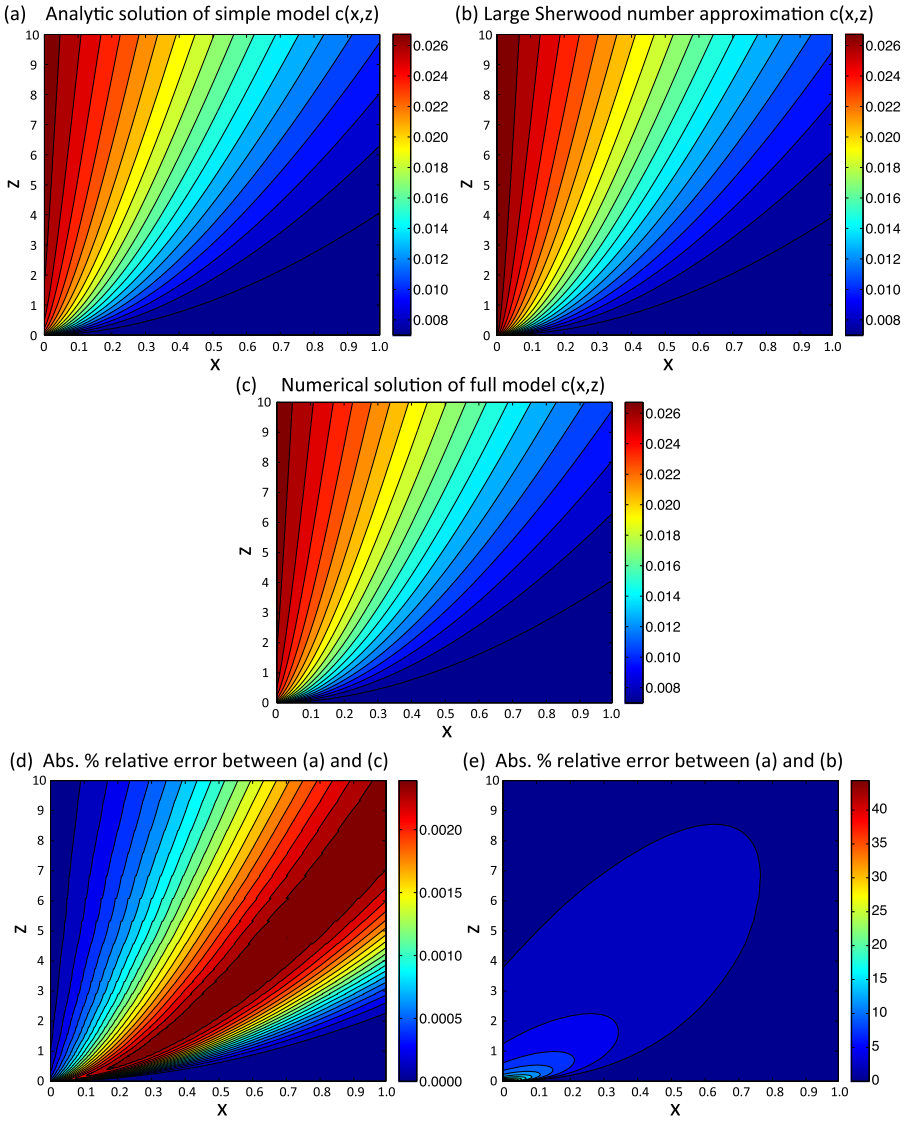

Figure 6 Analytic and numerical solutions to the simplified and full model as a function of *x* and *z*, with the relative errors between analytic and numerical solutions: (a) Analytic solution for the simplified model (32); **(b)** Large Sherwood number approximation (35), **(c)** Numerical solution of the full model (17), (18), (19) and (21), **(d)** Absolute value of the percentage relative error between the numerical solution of the full model and the analytic solution for the simplified model, **(e)** Absolute value of the percentage relative error between the Large Sherwood number approximation and the analytic solution for the simplified model. (Note the difference in scale for (d) and (e).)

main, convergence in terms of mesh size is relatively easy to ensure (see [42] for further details).

We see that the simplified model produces a solution that is very close (< 0.0025% error for the region we consider) to the more complete model. We can therefore conclude that the simplifying assumptions, that diffusion in the z-direction is neglected and that in the x-direction is constant, are reasonable for our set of parameter values. Even in the large Sherwood approximation the error is small if we are sufficiently far away from the point $x = 0$, $z = 0$, i.e. less than 10% error for $x > 0.15$, $z > 0.5$.

There are two further limits that we will explore: considering the concentration profile at the membrane, where $x = 0$, and close to the inlet at $z = 0$.

3.2 Near to the membrane: $x = 0$

The first case we consider is the easier of the two cases since we may simply substitute $x = 0$ into (32):

$$\begin{aligned} c(0,z) = c_0 + \frac{\sqrt{\delta}}{2} Sh\big(c^* - c_0\big) \int_0^z \exp\left(-\frac{\nu^2 u}{4\delta}\right) \\ \times \left\{ \frac{1}{\sqrt{\pi u}} - \gamma \exp\big(\gamma^2 u\big) \operatorname{erfc}(\gamma\sqrt{u}) \right\} \\ \times \left\{ \operatorname{erfc}\left(\frac{-\nu(z-u)}{2\sqrt{\delta(z-u)}}\right) + \operatorname{erfc}\left(\frac{\nu(z-u)}{2\sqrt{\delta(z-u)}}\right) \right\} du. \end{aligned} \tag{44}$$

However, $\operatorname{erfc}(u) = 1 - \operatorname{erf}(u)$ and erf is an odd function so $\operatorname{erfc}(u) + \operatorname{erfc}(-u) = 2$. Thus (44) becomes

$$\begin{aligned} c(0,z) = c_0 + \sqrt{\delta} Sh\big(c^* - c_0\big) \int_0^z \exp\left(-\frac{\nu^2 u}{4\delta}\right) \\ \times \left\{ \frac{1}{\sqrt{\pi u}} - \gamma \exp\big(\gamma^2 u\big) \operatorname{erfc}(\gamma\sqrt{u}) \right\} du, \end{aligned}$$

which, after interchanging the order of integration and a little manipulation, leads to

$$c(0,z) = c_0 + \frac{\sqrt{\delta} Sh(c^* - c_0)}{\gamma^2 - \alpha^2} \big\{ \gamma e^{(\gamma^2-\alpha^2)z} \big(\operatorname{erf}(\gamma\sqrt{z}) - 1\big) - \alpha \operatorname{erf}(\alpha\sqrt{z}) + \gamma \big\}, \tag{45}$$

where $\alpha = \nu/(2\sqrt{\delta})$. This solution is plotted in Figure 7 together with the full numerical solution. The agreement between the numerical solution and the analytic solution (45) is extremely good and the two plots are indistinguishable on this scale. The maximum percentage error between these two solutions is only 0.001%.

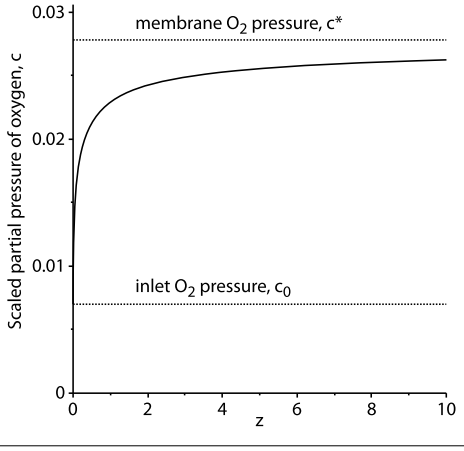

Figure 7 Non-dimensionalised oxygen partial pressure along the membrane at $x = 0$. Solid line is the analytical solution (45) and dashed line is numerical solution from the full model although these two lines are indistinguishable in this plot since the maximum percentage error is only 0.001%.

3.3 Near to the inlet: small z asymptotic expansion

Note that $z \ll 1$ implies (in (32)) that $u \ll 1$. If we also assume that $x/\sqrt{u} \gg 1$ when $u \ll 1$ then

$$\operatorname{erfc}\left(\pm\frac{\nu}{2}\sqrt{\frac{u}{\delta}} + \frac{x}{2\sqrt{\delta u}}\right) \sim \operatorname{erfc}\left(\frac{x}{2\sqrt{\delta u}}\right) \sim 2\sqrt{\frac{\delta u}{\pi x^2}}\exp\left(-\frac{x^2}{4\delta u}\right)\left(1 - \frac{2\delta u}{x^2}\right).$$

Thus, for $x \gg \sqrt{u}$ and $0 \le u < z \ll 1$,

$$\begin{aligned}&\operatorname{erfc}\left(-\frac{\nu}{2}\sqrt{\frac{u}{\delta}} + \frac{x}{2\sqrt{\delta u}}\right) + \exp\left(\frac{\nu x}{\delta}\right)\operatorname{erfc}\left(\frac{\nu}{2}\sqrt{\frac{u}{\delta}} + \frac{x}{2\sqrt{\delta u}}\right)\\ &\quad\sim 2\sqrt{\frac{\delta u}{\pi x^2}}\left(1 + \exp\left(\frac{\nu x}{\delta}\right)\right)\exp\left(-\frac{x^2}{4\delta u}\right)\left(1 - \frac{2\delta u}{x^2}\right).\end{aligned}$$

We further note that for $0 \le u < z \ll 1$,

$$\operatorname{erfc}(z) \sim 1 - \frac{2}{\sqrt{\pi}}z + O\left(z^3\right),$$

and $\exp(z) \sim 1 + O(z)$. Thus the complementary convolution of (32) allows us to write

$$\begin{aligned}c(x,z) \sim\ & c_0 + \frac{\delta}{x\sqrt{\pi}}Sh\left(c^* - c_0\right)\left[1 + \exp\left(\frac{\nu x}{\delta}\right)\right]\int_0^z \sqrt{u}\exp\left(-\frac{x^2}{2\delta u}\right)\\ &\times\left(1 - \frac{2\delta u}{x^2}\right)\left\{\frac{1}{\sqrt{\pi(z-u)}}\right.\\ &\left.-\gamma\left[1 - \frac{2}{\sqrt{\pi}}\left(\gamma\sqrt{(z-u)} + O\left((z-u)^{3/2}\right)\right)\right]\right\}du.\end{aligned} \tag{46}$$

Collecting terms of order z, $z^{3/2}$ and z^2 we obtain

$$\begin{aligned}c(x,z) \sim\ & c_0 + \frac{\delta}{x\sqrt{\pi}}Sh\left(c^* - c_0\right)\left[1 + \exp\left(\frac{\nu x}{\delta}\right)\right]\int_0^z \sqrt{u}\exp\left(-\frac{x^2}{2\delta u}\right)\\ &\times\left(\frac{1}{\sqrt{\pi(z-u)}} - \gamma + \frac{2\gamma^2}{\sqrt{\pi}}\sqrt{(z-u)} - \frac{2\delta u}{x^2\sqrt{\pi(z-u)}}\right)du.\end{aligned} \tag{47}$$

We first note that

$$\int_0^z \sqrt{u}\,du = \frac{2}{3}z^{3/2}, \qquad \int_0^z \sqrt{\frac{u}{z-u}}\,du = \frac{\pi}{2}z, \tag{48}$$

$$\int_0^z \sqrt{u(z-u)}\,du = \frac{\pi}{8}z^2, \qquad \int_0^z \sqrt{\frac{u^3}{z-u}}\,du = \frac{3\pi}{8}z^2. \tag{49}$$

Thus, by employing the mean value theorem for integrals, we obtain

$$\begin{aligned}c(x,z) \sim\ & c_0 + \frac{\delta}{x\sqrt{\pi}}Sh\left(c^* - c_0\right)\left[1 + \exp\left(\frac{\nu x}{\delta}\right)\right]\exp\left(-\frac{x^2}{4\delta z^*}\right)\\ &\times\left[\frac{1}{2}z - \frac{2\gamma}{3\sqrt{\pi}}z^{3/2} + \frac{1}{4}\left(\gamma^2 - \frac{3\delta}{x^2}\right)z^2\right],\end{aligned} \tag{50}$$

where $0 < z^* < z$. The expression (50), when plotted against the numerically obtained solution, does not compare favourably: this is almost certainly due to the slow convergence of the asymptotic expansion of the error function complement. Thus, this is not a particularly useful result. However, we do observe that, for z sufficiently small and $x = O(1)$, the concentration does grow linearly with z.

3.4 Large x and z asymptotics

If we now consider the situation for large z, so that the change is from $c = c^*$ close to the membrane) to $c = c_0$ far from the membrane, then we can approximate (22-24) to

$$\nu \frac{\partial c}{\partial x} + \frac{\partial c}{\partial z} = \delta \frac{\partial^2 c}{\partial x^2}, \tag{51}$$

$$c \to c_0, \quad \text{as } x \to \infty, \tag{52}$$

$$c \to c^*, \quad \text{as } z \to \infty. \tag{53}$$

If we translate to a moving frame, treating z as a time-like variable so that $X = x - \nu z$ and $T = z$, then we have

$$\frac{\partial c}{\partial T} = \delta \frac{\partial^2 c}{\partial X^2}, \tag{54}$$

$$c \to c_0, \quad \text{as } X \to \infty, \tag{55}$$

$$c \to c^*, \quad \text{as } X \to -\infty, \tag{56}$$

the classical diffusion equation. If we consider that the 'initial condition' at $T = 0$ is the function $c(X, 0) = c_0$ for $X > 0$ and $c(X, 0) = c^*$ for $X < 0$, then the solution is

$$c(X, T) = c_0 + \frac{(c^* - c_0)}{2}\left(1 - \operatorname{erf}\left(\frac{X}{\sqrt{4\delta T}}\right)\right), \tag{57}$$

or, in the original coordinate system,

$$c(x, z) = c_0 + \frac{(c^* - c_0)}{2}\left(1 - \operatorname{erf}\left(\frac{x - \nu z}{\sqrt{4\delta z}}\right)\right). \tag{58}$$

Figure 8(a) indicates a 'travelling wave' solution, with the concentration changing from c_0 to c^* with increasing z around the point $x \sim \nu z$. Figure 8(b) shows the manner in which the concentration changes, described by equation (58).

4 Device optimisation

An oxygenation device must re-oxygenate the blood entering the inlet by the time it leaves at the other end of the device. The longer the device the greater the amount of oxygen that can enter the blood. However, more compact devices are preferred, particularly if they are to be implanted, or portable. We would therefore like to reduce the length of the device while maintaining the oxygenation levels. We will concentrate on the oxygenation level at a fixed value $x = 1$, i.e. we consider a device of a nominal width of L.

Using the large Sherwood number solution, Figure 9(a) shows the oxygen partial pressure at $x = 1$ as a function of distance through the device, z, as we change the transverse

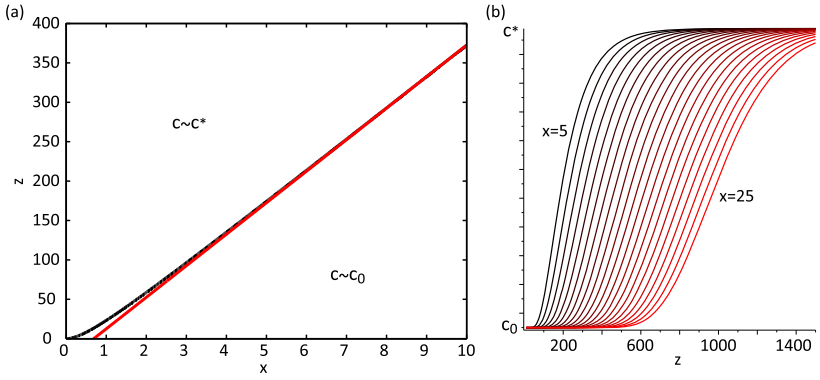

Figure 8 Plots of the large x and z asymptotics of the analytic solution showing the travelling wave behaviour: (a) Plot of the numerically obtained contour $c = (c^* + c_0)/2$ (black) and the line $z = z_0 + x/\nu$ (red). **(b)** Travelling wave concentration profiles for values of $x = 5$ (black) to $x = 25$ (red) as a function of distance z.

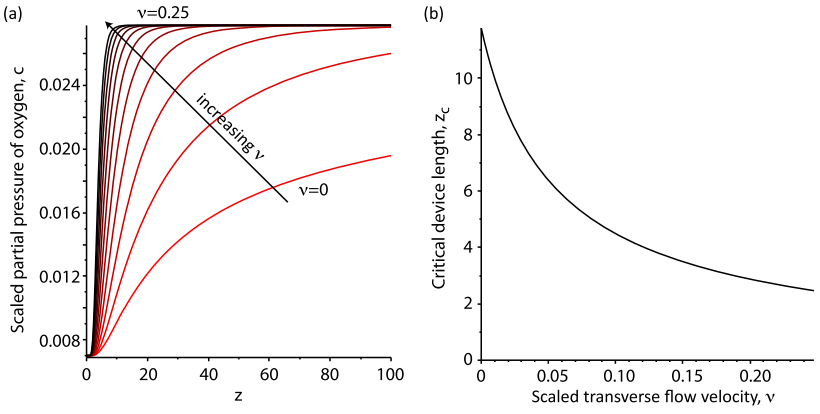

Figure 9 Example optimisation plots indicating the length of device and flow speed for which 90% saturation is achieved: (a) The oxygenation levels at $x = 1$ as a function of distance through the device z as the transverse flow speed ratio, ν, is varied **(b)** The critical length of the device to ensure the blood has reached 90% saturation at $x = 1$, as a function of transverse flow speed ratio, ν.

flow speed ratio ν. We see that, as we would expect, higher oxygenation levels are reached if the transverse flow is increased. Alternatively we can see that a fixed oxygenation level is reached at smaller values of z as transverse flow is increased.

If we assume that the device must increase the blood oxygenation level at all points of the outlet to at least 90% of the saturation level of blood then we must achieve $S = 0.9$ at $x = 1$. We denote the distance through the device at which $S = 0.9$ is achieved as z_c. Figure 9(b) shows the dependence of z_c on the transverse flow ratio. We see that even moderate values of transverse flow will significantly reduce the necessary length of the oxygenation device.

In fact we can find an implicit analytic form of the $z_c(\nu)$ function plotted in Figure 9(b). The value of c, say c_{Sc}, that ensures a particular saturation, say S_c, is derived from (18).

$$c_{S_c} = \left(\frac{S_c}{1 - S_c}\right)^{1/n} c_{0.5}. \tag{59}$$

Equation (35) can then be used to find the value of z_c at which this level of saturation is reached at a transverse location $x = x_L$

$$c_{S_c} = c_0 + \frac{1}{2}(c^* - c_0)\left\{\operatorname{erfc}\left(\frac{x_L - \nu z_c}{2\sqrt{\delta z_c}}\right) + \exp\left(\frac{x_L \nu}{\delta}\right)\operatorname{erfc}\left(\frac{x_L + \nu z_c}{2\sqrt{\delta z_c}}\right)\right\}. \tag{60}$$

This equation must in general be solved for z_c numerically, but such a numerical scheme will be significantly faster than any two- or three-dimensional solution of the full nonlinear model for the device flow and concentration profiles. The ability to obtain this final result, a semi-analytic solution for the distance z_c which is an indication of the length of device required, or other similar quantities derived from the analytic solution (35), is the justification for the simplifications made during the modelling stage. Using such results will assist a full device optimisation, that would inevitably involve a two- or three-dimensional model coupled with the solution of the Navier-Stokes equations and the equation of mass conservation for the fluid. In order to perform such an optimisation, it would be necessary to search over what might be a prohibitively large parameter space: the simple model provided in this paper will substantially reduce the region of search by indicating approximate parameter values that will deliver the required oxygenisation for a specific device geometry.

5 Conclusions

In this article we have provided a brief history of the artificial lung, or oxygen transfer device and described a mathematical model consisting of two coupled advection-diffusion-reaction equations. A number of simplifications and assumptions were made reducing the problem to a single stationary advection-diffusion equation which we then showed could be solved analytically using Laplace transforms and convolution. Some special cases were considered: large Sherwood number; solution close to the membrane ($x = 0$); solution near to the inlet (small z); and large x and z asymptotics. These results were then compared with a numerical solution of the original model and good agreement was obtained, justifying the assumptions and simplifications made. Thus predictions and some degree of device optimisation have been proposed as useful applications of the theoretical model.

Competing interests
The authors declare that they have no competing interests.

Authors' contributions
EAD carried out the experimental studies and wrote the initial draft of the manuscript. SM and NJM developed the mathematical model, with SM carrying out the mathematical analysis and NJM the numerical simulations and comparisons to analysis. SM and NJM drafted later versions of the manuscript and all authors read and approved the final manuscript.

Availability of data and materials
The dataset for Figure 3 is available in the University of Strathclyde KnowledgeBase repository, http://dx.doi.org/10.15129/a7f7374f-7220-4b13-8a5c-0267449cbe3d.

Author details
[1] Department of Mathematics & Statistics, University of Strathclyde, Livingstone Tower, Glasgow, G1 1XH, UK. [2] Golden Jubilee Foundation, Beardmore Street, Clydebank, Glasgow, G81 4HX, UK.

Acknowledgements
This work was partially funded by the UK Engineering and Physical Sciences Research Council Doctoral Training Centre in Medical Devices at the University of Strathclyde. The supervision and guidance of the late Dr John Gaylor, from the Department of Bioengineering at Strathclyde, was invaluable during this project.

Received: 9 July 2015 Accepted: 5 April 2016 Published online: 13 April 2016

References

1. von Schröder W. Uber die bildungstätte des harnstoffs. Arch Exp Pathol Pharmakol. 1882;15:364-402.
2. von Frey M, Grubber M. Ein respirations-apparat fur isolirte organe. Arch Physiol. 1885;9:519-32.
3. Gibbon JH Jr. An oxygenator with large surface area to volume ratio. Clin Chem Lab Med. 1939;24:1192-8.
4. Kirklin JW, Donald DE, Harshbager HG, Hetzel PS, Patrick RT, Swan HJC, Wood EG. Studies in extracorporeal circulation. I. Applicability of Gibbon-type pump-oxygenator to human intracardiac surgery: 40 cases. Ann Surg. 1956;144:2-8.
5. Burns N. Production of a silicon rubber film for the membrane lung. Biomed Eng. 1969;4:356-9.
6. Burns N, Melrose D. An improved silicone membrane. Adv Cardiol. 1971;6:58-71.
7. Weissman MH, Mockros LF. Oxygen transfer to blood flowing in round tubes. J Eng Mech Div. 1967;93(6):225-44.
8. Dindorf JA, Lightfoot EN, Solen KA. Prediction of blood oxygenation rates. Chem Eng Prog Symp Ser. 1971;114(67):75-87.
9. Colton CK, Drake RF. Effect of boundary conditions on oxygen transport to blood flowing in a tube. Chem Eng Prog Symp Ser. 1971;114(67):88-95.
10. Spaeth EE. Blood oxygenation in extracorporeal devices: theoretical considerations. CRC Crit Rev Bioeng. 1973;1:383-417.
11. Eberhart RC, Dengle SK, Curtis RM. Mathematical and experimental methods for design and evaluation of membrane oxygenators. Artif Organs 1978;2(1):19-34.
12. Jayaraman G, Lautier A, Jarry G, Bui-Mong-Hung, Laurtent D. Numerical scheme for modelling oxygen transfer in tubular oxygenators. Med Biol Eng Comput 1981;19:524-34.
13. Mayes PJD. An application of the method of lines in biological mass transfer. Biotechnol Prog. 1985;1(4):269-72.
14. Vaslef SN, Mockros LF, Cook KE, Leonard RJ, Sung JC, Anderson RW. Computer-assisted design of an implantable, intrathoracic artificial lung. Artif Organs. 1994;18(11):813-7.
15. Zierenberg JR, Hirschi RB, Grotberg JB, Bartlett RH, Fujioka H. Pulsatile blood flow and oxygen transport past a circular cylinder. J Biomech Eng. 2007;129(2):202-15.
16. Taskin ME, Fraser KH, Zhang T, Griffith BP, Wu ZJ. Micro-scale modelling of flow and oxygen transfer in hollow fibre membrane bundle. J Membr Sci. 2010;362(1-2):172-83.
17. Hewitt TJ, Hattler BF, Federspiel WJ. A mathematical model of gas exchange in an intravenous membrane oxygenator. Ann Biomed Eng. 1998;26:166-78.
18. Suitek RG, Federspiel WJ. A mathematical model to predict CO_2 removal in hollow fibre membrane oxygenators. Ann Biomed Eng. 2008;36(6):992-1003.
19. Potkay JA. A simple, closed form, mathematical model for gas exchange in microchannel artificial lungs. Biomed Microdevices. 2013;15:397-406.
20. Whiteley JP, Gavaghan DJ, Hahn CEW. Mathematical modelling of pulmonary gas transport. J Math Biol. 2003;47:79-99.
21. Whiteley UP, Gavaghan DJ, Hahn CEW. Some factors affecting oxygen uptake by red blood cells in the pulmonary capillaries. Math Biosci. 2001;169:153-72.
22. Vadapalli A, Goldman D, Popel AS. Calculations of oxygen transport by red blood cells and haemoglobin solutions in capillaries. Artif Cells Blood Substit Immobil Biotechnol. 2002;30(3):157-88.
23. Caputo M, Chiastra C, Cianciolo C, Cutri E, Dubini G, Gunn J, Keller B, Migliavacca F, Zunino P. Simulation of oxygen transfer in stented arteries and correlation with in-stent restenosis. Int J Numer Methods Biomed Eng. 2013;29:1373-87.
24. Formaggia L, Nobile F, Quarteroni A, Veneziani A, Zunino P. Advances on numerical modelling of blood flow problems. In: European Congress on Computational Methods in Applied Sciences and Engineering (ECCOMAS 2000), 11-14 September, Barcelona. 2000.
25. Formaggia L, Quarteroni A, Veneziani A. Cardiovascular mathematics: modeling and simulation of the circulatory system. Mailand: Springer; 2009.
26. Dougall EA. Investigation of oxygen transfer in novel medical devices. PhD thesis, University of Strathclyde. 2011.
27. COMSOL Multiphysics. 2013. version 4.3b, COMSOL Inc.
28. Van Genuchten, Th M, Alves WJ. Analytical solutions of the one-dimensional convective-dispersive solute transport equation. Technical Bulletin No. 1661, U.S. Department of Agriculture. 1982.
29. Yuan F, Lu Z. Analytical solutions for vertical flow in unsaturated, rooted soils with variable surface fluxes. Vadose Zone J. 2005;4:1210-8.
30. McKay C, McKee S, Mulholland AJ. Modelling deposition of a pollutant from a chimney stack. IMA J Appl Math. 2006;71:670-91.
31. Kumar A, Jaiswal DK, Kumar N. Analytical solutions of one-dimensional advection-diffusion equation with variable coefficients in a finite domain. J Earth Syst Sci Educ. 2009;118(5):539-49.
32. Jaiswal DK, Kumar A. Analytical solutions of time and spatially dependent one-dimensional advection-diffusion equation. Elixir Poll. 2011;32:2078-83.
33. McGinty S, McKee S, Wadsworth RW, McCormick C. Modelling arterial wall drug concentrations following the insertion of a drug-eluting stent. SIAM J Appl Math. 2013;73(6):2004-28.
34. Pontrelli G, de Monte F. A multi-layer porour wall model for coronary drug-eluting stents. Int J Heat Mass Transf. 2010;53(1):3629-37.
35. Pedley TJ. The fluid mechanics of large blood vessels. Cambridge: Cambridge University Press; 1980.
36. Berman J, Markros LF. Mass transfer to fluids flowing through non-aligned straight tubes. J Biomech Eng. 2009;108(4):342-9.
37. Gaylor JDS. Membrane oxygenators: current developments in design and application. J Biomed Eng. 1988;10:541-7.
38. Dorrington KL. Anaesthetic and extracorporeal gas transfer. Oxford: Clarendon Press; 1989. p. 203-38.
39. Doetsch G. Introduction to the theory and application of Laplace transforms. Berlin: Springer; 1974.
40. McGinty S, McKee S, McCormick C, Wheel M. Release mechanisms and parameter estimation in drug-eluting stent systems: analytical solutions of drug release and tissue transport. Math Med Biol. 2015;32(2):163-86
41. Abramowitz M, Stegun I. Handbook of mathematical functions. New York: Dover Publications; 1970.
42. Zimmerman WBJ. Multiphysics modeling with finite element methods. Singapore: World Scientific; 2006.